Published in final edited form as:
Anal Chem. 2013 November 5; 85(21): . doi:10.1021/ac402383n.

Self-Digitization of Samples into a High-Density Microfluidic Bottom-Well Array

Thomas Schneider, **Gloria S. Yen**, **Alison M. Thompson**, **Daniel R. Burnham**, and **Daniel T. Chiu**
Department of Chemistry, University of Washington, Seattle, WA 98195-1700, USA.

Abstract

This paper describes a sample digitization method that generates tens of thousands of nanoliter-sized droplets in a high-density array in a matter of minutes. We show that the sample digitization depends on both the geometric design of the microfluidic device and the viscoelastic forces between the aqueous sample and a continuous oil phase. Our design avoids sample loss: Samples are split into tens of thousands of discreet volumes with close to 100% efficiency without the need for any expensive valving or pumping systems. We envision this technology will have broad applications that require simple sample digitization within minutes, such as digital polymerase chain reactions and single-cell studies.

INTRODUCTION

Droplet microfluidics is a technology that allows an aqueous sample to be compartmentalized into individual droplets. When applied to chemical and biological analyses, droplet microfluidics has the potential to reduce costs by minimizing the amount of reagents required and improving the performance statistics of the analytical techniques by assessing thousands of droplets at high sensitivity over a short time period. In the past decade, various methods have been developed to generate droplets in flow on microfluidic platforms. Among the most popular methods are in-flow methods based on hydrodynamic flow focusing [1] and the geometrically induced droplet breakup at T-junctions. [2] The simplicity of these methods led to seminal advances in the study of mixing [3, 4], the generation of multiemulsion droplets [5, 6], in electrophoretic separations [7, 8], the encapsulation of whole cells [9, 10,] and the use of these cells for the study of gene, enzyme, or protein expressions [11-16], cell cultivation [17], and drug screening. [18, 19] The interested reader is referred to the numerous well-written summaries on the state-of-the-art in droplet microfluidics. [20-24]

While these droplet microfluidic methods can generate droplets easily in the range of kHz[15], the detection, monitoring, and addressability of individual droplets in a steady-state continuous-flow fashion can be challenging. To address these challenges, we recently presented a simple and robust method for spontaneously generating large arrays of small sample volumes. [24-26] We called this method "self digitization" (SD) because the process occurs spontaneously and is based on viscoelastic fluid phenomena driven by the geometric properties of a microfluidic channel. [25]

chiu@chem.washington.edu.

Conflict of Interest
The authors declare the following competing financial interest(s): D.T.C. has financial interest in Lamprogen, which has licensed the described technology from the University of Washington.

In our present study, we introduce sample self-digitization in a high-density array of microfluidic wells fabricated into the bottom of the channels. Our previous fluidic design for carrying out sample self-digitization was based on a series of side chambers set off from the main microfluidic channel. However, SD chips with wells below the channels can be advantageous over the side-chamber design because wells at the bottom of the main channel can: *i*) provide denser arrays per chip area, *ii*) allow one to interact with the digitized droplet in a top-down configuration commonly used in microscopy techniques (*e.g.*, optical tweezers [27], biomagnetic separations [28-30], or mechanical actuators [31]), and *iii*) the confined droplets are separated from the device's polymeric material by a thin layer of oil present in the main channel. This is beneficial not only for separating adjacent compartmentalized aqueous samples, but can also provide a barrier that prevents evaporation of sample components during thermal heating (*e.g.*, during a digital polymerase chain reaction (PCR) or when used as a micro-bioreactor for single cells studies).

Despite the appeal of digitizing a sample into an array of wells at the bottom of microfluidic channels, this feat is difficult to achieve. For example, extremely poor or no digitization occurred when we used bottom-well arrays connected to a large open channel or when the width of the channel has the same width as the well (Fig. 1b). We found digitization only adequately worked when certain fairly stringent geometric parameters are met, for example, when the width of each well was slightly narrower than the width of the main channel on top, and the height of the main channel also had to be shallow, which helped to drive the aqueous solution into the bottom well to displace the oil present in the well. To better understand the importance of both the geometric factors and fluid properties in sample digitization, we carried out on-chip experiments as well as three-dimensional computational fluid dynamics (CFD) simulations. Our studies were conducted on microfluidic chips with arrays ranging from 1,024 to 38,400 wells where the well volumes were 1-2 nL. The results of sample digitization with the on-chip experiments agreed mostly with those obtained from three-dimensional CFD studies. We envision this ability to digitize an aqueous sample into a large array of immobilized discrete volumes will find use in digital-biology measurements, such as digital PCR and single-cell analysis.

EXPERIMENTAL SECTION

Microchip Fabrication. Microfluidic chips were based on arrays of wells with width (w = 100 to 200 μm), length (l = 100 to 200 μm), and depth (d = 100 μm) connected to a main channel above them of height (H_m) and width ($W_m = w + 2W$), where W is the channel's overhang with respect to the bottom well (Fig. 1). The well volume (V_w) was chosen to be between 1 and 2 nL in all experiments. For the study, we varied the main channel's dimensions by changing W from 0 to 25, 50 and 100 μm and the well spacing (δ) from 50 to 100 and 200 μm, while H was 20 μm in all experiments. The main channel geometry was further modified to incorporate constrictions of width (W_c) and length (l_c) before and after each well at a distance of δ_c. Sketches in Fig. 1 illustrate how the design of the chip evolved. Arrays of 1,024 wells were used for the parametric investigations. Larger area chips with up to 38,400 wells per chip (V_w = 2 nL) were used in the scale up studies.

The microfluidic chips were fabricated by multilayer soft photolithography [32] on 3-inch silicon wafers (300-400 μm thick, reclaim; Montco Silicon Technologies, Inc., Spring City, PA) using an epoxy-based negative photoresist (SU-8; MicroChem Corp., Newton, MA). The feature heights were subsequently measured by a custom-built white-light interferometer. [33] Finally, the feature masters and an empty silicon wafer were cleaned with ethanol (200 proof; Decon Laboratories, Inc.; King of Prussia, PA) and silanized (tridecafluoro-1,1,2,2-30 tetrahydrooctyl trichlorosilane; Gelest Inc., Morrisville, PA) under vacuum and overnight.

The microfluidic structures were subsequently cast in PDMS (SYLGARD® 184 Silicone Elastomer Kit, Dow Corning, Corp., Midland, MI). A flat PDMS slab for the inlet/outlet ports was separately cast on a featureless and silanized wafer. After the PDMS pieces were removed from the masters, inlet and outlet ports were cut into the featureless PDMS slab, cleaned with ethanol and blow-dried with N_2 gas. The two PDMS pieces were then placed inside a plasma cleaner (Expanded Plasma Cleaner/Sterilizer; Harrick Plasma, Ithaca, NY). The plasma cleaner was evacuated thrice (< 100 mTorr) followed by purging with O_2. After the last purge with O_2 and following evacuation below 160 mTorr, the plasma was initiated at high level and left on for 45 seconds. The two PDMS pieces were brought in close contact immediately after removal from the plasma cleaner. Finally, the PDMS pieces were placed at 110-115°C for 24 hours to allow the PDMS to revert back to its hydrophobic character.

Sample Preparation

Silicone oil (50 cSt; cat. 378356; Sigma Aldrich, Inc., St. Louis, MO), mineral oil (30.0 cSt; light, embryo tested; cat. M8410; Sigma Aldrich, Inc.), and mixtures of the oils with hexadecane (Sigma Aldrich, Inc.) were used as the oil phase. The silicone oil and mineral oil were supplemented with surfactants of 0.01%$_{w/w}$ (Gransurf 77; Grant Industries, Inc., Elmwood Park, NJ) and 0.02% (Span 80; Sorbitan monooleate, Sigma Aldrich, Inc.), respectively. Highly purified water (MilliQ; Millipore Corp., Billercia, MA) supplemented with 100 μM Fluorescein (Reference Standard; cat. # F-1300; Molecular Probes, Invitrogen Corporation, Carlsbad, CA) was used as the aqueous solution.

Sample Digitization

Before sample digitization, a long plug of aqueous solution was sandwiched between the oil phase by aspirating both samples sequentially into PTFE tubing (20G PTFE; cat #50806; Zeus Industrial Products, Inc., Orangeburg, SC). The aqueous plug had a volume of at least 1.5-times the chip volume. The tubing was connected to the chip's inlet by metal interconnectors (20G ½" blunt, 45°; cat.# NE4520-6; Small Parts, Inc., Miramar, FL) and to pressurized air by LUER connectors (Upchurch Scientific, Inc., Oak Harbor, WA). The air pressure was supplied by a compressor (Panther, # P100-24AL/M07090; Werther International Inc., Houston, TX) and regulated by a pressure gauge (0-100 psi, AR91-100; Omega Engineering, Inc., Stamford, CT).

The chip filling and digitization was visualized by a wide-area microscope (AZ100 Multizoom; Nikon Inc., Melville, NY; Zoom Stereo Microscope SZ61; Olympus Imaging America Inc.; Center Valley, PA) equipped with a 1× and 4× objective (NA: 0.1/WD: 35mm and NA: 0.4/WD: 20mm, respectively; Nikon Inc.) in bright field and under fluorescence excitation (FF01–482/35–25, FF01–536/40–25; SEMROCK Brightline, IDEX Corp., Rochester, NY). Images were acquired using a CCD camera (GC1380; Allied Vision Technologies Canada Inc., Burnaby, B.C., Canada) and custom-coded acquisition software (LabVIEW v8.6; National Instruments Corporation, Austin, TX).

Computational Fluid Dynamics (CFD) of Sample Digitization

Three-dimensional multiphase fluid simulations of the sample digitization in single bottom wells were conducted with a CFD package (Fluent, Version 6.3.26; Fluent Inc.; ANSYS, Inc., Lebanon, NH). The droplet digitization was simulated for different viscous/interfacial properties (Ca) and varying dimensions of the main channel (W_m, H_m) with a bottom well measuring 100 μm × 200 μm × 100 μm ($w \times l \times d$). The designs were converted into finite elements using a hexahedral meshing strategy with a resolution of 2.5 – 5.0 μm between node points. In all simulations, water ($\rho = 998$ kg m^{-3}, $\mu = 1.003\times10^{-3}$ kg m^{-1}s^{-1}) and silicone oil (50 cSt; $\rho = 980$ kg m^{-3}, $\mu = 0.049$ kg m^{-1} s^{-1}) were used as aqueous solution and oil phase, respectively. The model solver was defined as pressure-based, three-

dimensional, with an absolute velocity formulation, and a first-order implicit unsteady formulation with non-iterative time advancement.

A volume of fluid (VOF) solver was used for the multiphase model with two phases, explicit VOF scheme, and a Courant number of 0.25. The phase interaction was defined with wall adhesion properties and different γ values for the water-oil interface ranging from 5-30 mN m^{-1}. The boundary conditions were set as follows: The single inlet was defined by a flat velocity profile depending on the parameter studied; the outlet was defined as outflow with a constant pressure ($P_{Outlet} = P_{atm} = 101325$ Pa); the walls enclosing the main channel and well were set to have a hydrophobic contact angle of 175°. The main channel and bottom well were then prefilled with the oil phase and aqueous solution using Fluent's "Adapt" tool resulting in an aqueous plug with a volume of 1.5 – 2.0 times the well volume and reaching up to 25 Bm before the well. The fluid flow profile and the volume fractions were then simulated with fractional steps for the pressure-velocity coupling. The spatial discretization was implemented by a first-order upwind scheme for the momentum and a pressure staggering option (PRESTO!) set for the pressure. The volume fraction was discretized using the Geo-Reconstruct option. All residual tolerances were set to 0.001. The simulations were subsequently iterated with time steps ranging from 0.1 to 5.0 μs.

Data Analysis & Statistics

The data analysis was conducted from fluorescence images of the entire SD Chip. A custom matching algorithm was used to stitch together individual images taken from chips with large areas (LabVIEW v8.6; National Instruments Corporation). A separate custom LabVIEW program was then used to analyze the fluorescence image using blob analysis [34], a user specified well size (taken from the bright field images), and two different thresholding schemes. The 8-bit images of the fluorescent aqueous solution retained in the wells and main channels showed different grey levels. The fluorescent sample in the thin main channel had much lower pixel grey level intensities than the fluorescent samples in the deeper bottom wells. This difference in grey level intensities allowed two thresholding schemes for the analysis. These thresholding schemes were used to calculate *i*) the digitization or filling efficiency and *ii*) the retention ratio. The filling efficiency is based on the analysis at low threshold of individual digitized samples (*i.e.*, accounting for wells that remained interconnected by a bridge of aqueous solution in the main channel). The retention ratio is based on the image analysis at high threshold to account for the total number of wells filled or retained per chip, regardless of connections of the wells to the main channel by the aqueous solution. Therefore, our analysis and data representation will be based on *i*) the fraction of individually digitized samples per chip (digitization or filling efficiency, f_{total}), and based on *ii*) the total sample retention per chip, R_{total}.

Results and Discussion

Sample Retention and Total Digitization or Filling Efficiency

The sample self digitization in these SD chips occurs in wells below the main microfluidic channel - we call the device a bottom-well array to distinguish it from the side-chamber geometry that we reported previously. [25, 26] The self-digitization is based on the interplay between viscoelastic forces and the geometries of the main channel and the wells. A schematic of the self-digitization in an oil-filled channel is shown in Fig. 1a. After priming the channel with oil (light blue), the aqueous solution (dark blue) was pumped into the channel and sheared off by the oil phase. To study the experimental parameters required to achieve high digitization efficiency and sample retention, we began by investigating the use of straight main channels. Subsequent design optimizations led to the use of constrictions and variations to the outlet drainage channels; these optimizations achieved high digitization

efficiencies during scale-up of the number of wells below the main microfluidic channel in a chip. The evolution of the design is sketched in Fig. 1c-e.

The self-digitization of sample volumes in chips with wells below straight main channels showed a strong dependence on the main channel's dimensions and capillary number (*Ca*). We conducted an extensive study with arrays of 1,024 wells per chip to investigate different parameters that affected the filling and digitization. These parameters included the main channel's overhang with respect to the well width (*W*/*w*), the normalized spacing between wells (δ/w), and the aspect ratio of the well with respect to the flow direction (*l*/*w*). The results from the parameter study were based on fluorescence microscopy images of filled wells (bright in Fig. 2a) with respect to the oil-filled, non-fluorescent chip (black in Fig. 2a). The results are presented as the retention ratio (*R*) and the total filling (or digitization) efficiency (f_{total}). The retention ratio is defined as the number of wells filled per chip, independent of wells that remain connected to the main channel (as the connection through the main channel is filtered out by the thresholding scheme), and is normalized to the total number of wells per chip. In contrast, the filling efficiency or digitization efficiency accounts for wells which remain connected by an aqueous bridge through the main channel. An aqueous sample that spreads over several wells and remains connected through the main channel is treated as one droplet. The filling efficiency is also normalized by the total number of wells per chip. A filling efficiency of 1 represents the filling of the entire chip with aqueous samples occupying single wells without any interconnection through the main channel to neighboring wells (perfect digitization). With decreasing filling efficiency, the fraction of aqueous samples that are larger in volume than a single well is increasing (*e.g.*, as a result of an aqueous bridge connecting neighboring wells). Therefore, the retention ratio tells us how many wells per SD chip are filled with aqueous sample and the filling efficiency is a measure of the quality of the digitization (*i.e.*, low *f* corresponds to many interconnected droplets and high *f* corresponds to a few to none). The goal of the study was to achieve complete filling of the entire chip with digitized aqueous samples each with a volume of a single well.

Our experimental study showed that more than 50% in sample retention was achieved for the entire range of channel overhang (*W*) and *Ca* range studied, except for the highest *Ca* and *W*/*w* (right panel in Fig. 2c). At the same time, the filling efficiency appeared to be decreasing with increasing *W*/*w* (left panel in Fig. 2c). In experimental studies with supposedly no overhang (*W*/*w* of 0), the filling efficiency showed an increase with increasing *Ca*. For larger values of *W*/*w*, this trend was not as clear, which suggested a more complex interplay between *Ca* and channel dimensions than could be explained by a single parameter such as *W*/*w*. Overall, it can be expected that the filling efficiency decreased with decreasing *Ca* and increasing *W*/*w*. This is due to higher shear flow of the oil phase in thinner channels (low *W*/*w*) when compared to wider channels (high *W*/*w*). For the parameter *W*/*w*, we found in our experiments that relatively high sample retention and filling efficiency was achieved for *W*/*w* values of 0 to 0.5 and for high *Ca* (0.02 – 0.03). High *Ca* values used during digitization were also beneficial to minimize the time required to fill and digitize a chip because *Ca* is directly proportional to the linear flow velocity of the oil phase. However, at the highest *Ca* studied, the shear flow resulted in the generation of many small emulsified droplets per well and artificially raised the filling efficiency above the calculated retention (Fig. 2c). This emulsification was only seen for the parameter with supposedly no overhang and high *Ca*.

CFD simulations of the sample digitization showed that actually no sample was retained when there was no overhang, that is, when *W*/*w* = 0, except when *Ca* was very low (see circle symbols in Fig. 2g). The simulations also indicated that a small *W* was required to allow for samples to be digitized and retained. This simulation result contrasted with our on

chip experiments described above, which showed sample retention even when W/w was supposedly 0 (Fig. 2c). This apparent contradiction could be explained by imperfections in the multi-layer microfabrication process. Minor misalignments in the fabrication process between the first layer (main channel) and the second layer containing the wells could result in edges that supported droplet retention. Indeed, we noticed that a ~1-2 μm misalignment, as measured by bright field microscopy, was present in our master that supposedly should not have any overhang; this slight misalignment was difficult to overcome with our fabrication process. From our simulations, this slight overhang would have allowed for sample digitization into the wells, consistent with our experimental observations.

In contrast, a larger W reversed the effect of high filling efficiency, which was explained by the way the bulk aqueous solution was digitized in each well (Fig. 2a,b). The aqueous compartment in each well was pinched off from the bulk aqueous solution by the shearing of the oil phase between adjacent wells. Wider main channels resulted in weaker shear forces, thus reducing the pinching of the aqueous droplet after it filled in the well; as a result, aqueous droplets in adjacent wells remained interconnected by an aqueous bridge in the main channel, which also increased the chances that they became dislodged from the wells by flow in the main channel.

Based on the results from the overhang study (W/w), it is tempting to argue that a large inter-well spacing (δ) may be beneficial to facilitate digitization and achieve high sample retention and filling efficiency. In order to investigate the impact of well spacing, we fixed W/w at 0.5 and normalized the results for different δ to the well width. From the computational analysis that indicated the requirement for a small overhang and based on the R_{total} and f_{total} results on-chip, we chose the fixed value of W/w. Our on-chip results showed that a small δ/w resulted in high sample retention for the Ca range studied, albeit for a decrease in R_{total} with increasing Ca (Fig. 2d). The results for large δ/w showed a pronounced impact of the Ca on sample retention. Here, small Ca allowed the retention of the aqueous sample while at large Ca (≥0.02), the aqueous sample was flushed out of the SD chip. Not as clear was the trend in filling efficiency for studied q/w and Ca range. At small δ/w and low Ca, there was a low f_{total}, indicating that many of the aqueous compartments remained interconnected through bridges between adjacent wells. The use of higher Ca, and thus higher shear rates of the oil phase, allowed for increasing the filling efficiencies. But these increases were limited to low δ/w. These results indicated that δ has similar effects on the breakup of individual droplets from the bulk aqueous solution as the main channel overhang (*i.e.*, by nicking or pinching during shearing by the oil phase). A small δ tended to support digitization of well sized aqueous droplets while large δ led to strongly reduced sample retention. Furthermore, the interwell spacing had a strong impact on the density of wells located below a microfluidic channel. Larger interwell spacing reduced the overall sample volume that could be digitized or retained in a chip for a given chip area.

Another parameter which affected sample retention was the well length (l), which was in the direction of the main channel flow. For W/w of 0.5, we found that l/w of 0.5 (*i.e.*, a wide well perpendicular to the flow direction) was least beneficial for high f_{total} and R_{total}. Wells with a square cross-section (l/w of 1.0) showed higher f_{total} and R_{total} with increasing Ca. The overall trend in sample digitization and retention suggested a rectangular well placed in the flow direction (l/w) was most beneficial for high f_{total} and R_{total} (Fig. 2e).

To highlight the importance of Ca on the sample retention, we combined all the data from the parametric study into a single plot (Fig. 2f). The plot shows there was a distinct trend in the retention of sample (R_{total}) with increasing Ca. Almost 100% of the sample could be retained in the chip at a Ca smaller than 0.020. At higher Ca, the majority of the aqueous sample was flushed out of the chip by the shearing oil phase, thus decreasing R_{total}.

Improvements of Sample Digitization and Effect of Main-Channel Height

CFD was shown to be a powerful tool to study process parameters for our side chamber SD chips. [25] A similar approach was used to investigate parameters that can improve the sample digitization in SD chips with wells below the main channel. Preliminary simulation and experimental studies with bottom well SD chips with varying main-channel heights (H_m) indicated a critical height above which the sample digitization was greatly reduced. In these studies, bottom well SD chips with well volumes of 2 nL were used. These chips had a normalized channel overhang (W/w) of 0.25, a normalized well spacing (δ/w) of 0.5, and a well aspect ratio (l/w) of 2.0. The experimental studies indicated that R_{total} and f_{total} approached zero when H_m was greater than 30-40 μm. To further investigate the effects of main channel geometry and changes in Ca on the sample digitization, we used CFD models to simulate the filling of a single well. An example of the CFD study is shown in Fig. 2b with the stages before and during well filling with aqueous solution (t_0, t_1) and after shearing by the oil phase (t_2). The material properties (oil and water) used in on-chip experiments were also used in the CFD studies. Unlike the on-chip studies, the CFD study allowed for the direct readout of the retained aqueous sample volume; the results are presented normalized to the well volume, V_w, in the Ca plot (Fig. 2g).

In the studies with a main channel height of 25 Bm (open symbols in Fig. 2g), we found that the V/V_w decreased with increasing Ca and approached zero at Ca of 0.020 (except for studies with $W/w = 0$). Furthermore, with increasing W/w, the ratio of retained sample volume increased. At a W/w of 0, the sample was only retained at low Ca. This result indicates the requirement for a small main channel overhang to allow the sample to be retained in the well. When the Ca was used as an indicator for retention or no retention of sample in the well, the overall trend was found to be similar between the on-chip and CFD data shown in Fig. 2. The change in volume of the retained droplet could only be directly quantified by the CFD data. Therefore, it must be noted that the retention data shown in Fig. 2f was based on the samples' cross-sectional area, while in Fig. 2g, the entire sample volume of the retained droplet was taken into account.

When H_m increased to 50 Bm (grey symbols in Fig. 2g), we found that a larger fraction of the digitized sample expanded into the main channel, as the sample droplet filled out the main channel volume above the well (therefore $V/V_w >> 1.0$). The sample retention abruptly approached zero at a much lower Ca (~0.0065) when compared to H_m of 25 μm (retention below Ca of 0.020). However, at $W/w < 0.25$, none of the aqueous sample was retained in the well when H_m was 50 μm and for the Ca range used in the CFD study ($Ca = 0.0016 – 0.0196$).

The results from the CFD study for variations in main channel height indicated that the sample retention and sample digitization were not only dependent on the main channel's overhang (W), but also were greatly affected by the main channel's height. This observation suggested that the pinching of the aqueous solution by the shearing oil phase was dominated by the main channel geometry (H_m and W_m). The data also show that if H_m exceeded a critical value, none of the aqueous solution sample could be digitized.

Maximizing f_{total} and R_{total} for SD chip scale-up

So far, our study showed that for chips with 1,024 wells, the parameters for the main channel's geometry were the ones that could be optimized to achieve sample retention and digitization efficiencies of 80-90%. Additional parameters were introduced to further improve and maximize f_{total} and R_{total}. These parameters included the use of constrictions before and after each well; the design evolution of these changes are shown in Fig. 1c-e. The modifications to the main channel design were based on simulation and experimental

observations of the aqueous sample breakup during shearing by the oil phase and were aimed at improving the pinching mechanism between adjacent wells (Fig. 2a,b). The chips with 1,024 wells used for the parametric study employed bifurcations to connect the parallel main channels to a single inlet and single outlet. We found that during scale up of the well numbers per chip, the bifurcation of the outlet channels resulted in strong interactions between neighboring channels and affected sample retention and digitization efficiency. To minimize cross-talk or reversed sample flow between channels, all channels were connected via a small fluidic resistor (*i.e.,* a narrow channel) to a large outlet reservoir. This change in the design of the main channel outlet greatly improved the drainage of the oil phase from the main channel and allowed for a much faster sample digitization; a feature important for chips with tens of thousands of wells. Additionally, the use of hexadecane mixed with the oil phase in a ratio of 1:1 or 1:2 was used to reduce the oil phase viscosity and helped to improve digitization efficiency in chips with more wells.

We investigated the effect of scale up in chips with up to 38,400 wells per chip (V_{well} = 2 nL). Tight constrictions ($W_c = ⅓ W_m$) and the tapering off of the wells in the flow direction (Fig. 1e) resulted in improved pinching of the aqueous solution during shearing by the oil phase. A typical filling result of a bottom-well chip with 4,096 and 38,400 wells of approximately 2 nL per well is shown in Fig. 3a. Overall, the sample retention and filling efficiencies in these studies were between 95-100% and showed minimal dependence on the various chip sizes (Fig. 3b). The time required for digitization of an aqueous sample in these chips was found to be dependent on the total number of wells per chip and the sample properties (*i.e.,* oil phase viscosity, surfactant concentration), but was generally in the minutes range.

For the 38,400-well chip, further improvements can be achieved by using more advanced microfabrication methods, such as silicon micromachining. The chips used in our study were based on replicas from masters created by soft lithography. Soft lithography is an ideal method for conceptual studies as it allows quick turnaround times between design iterations and is relatively cheap. However, a drawback of soft lithography is the challenge of creating feature masters that are both dense in their structures and large in area. The losses in sample retention especially in chips with larger areas such as those with 38,400 wells per chip were found to be at the edges of these chips and close to the outlet (see Fig 3a). Such edge effects were gradually reduced by optimizing the outlet section and outflow of the sample. The 38,400-well chip used in our study was replicated from a dense and large area feature master that contained some imperfections (*e.g.,* slight variations in heights of the main channel and depths of well). Although the imperfections in fabrication of our feature masters were limited in number, they could lead to localized variations in the flow profile and affect the overall filling efficiency and sample retention. The use of sophisticated micromachining techniques, albeit currently costly on the large scale, is expected to minimize, if not eliminate, imperfections of the master wafer and result in better performance of the SD chip.

Conclusion

A new generation of SD chips was developed and optimized for nearly 100 percent digitization of sample volumes in highly dense arrays in wells at the bottom of microfluidic channels. The microarrays presented in this study allowed for the self-digitization of sample volumes in a way similar to that presented in our recent study with microfluidic side chambers. [25] However, the bottom wells in this current work have more attractive features than the side chambers for a wider range of potential applications: One advantage is the potential for higher well densities, which allow larger sample volumes to be compartmentalized per chip for a given area. We conducted a parametric study with arrays of 1,024 wells and straight main channels to investigate how the geometric parameters of the

microfluidic chip and viscous/interfacial forces of the sample solutions affected the retention and digitization of individual samples per well. We found that a flat and straight main channel with a slight overhang in combination with closely spaced bottom wells can give rise to nearly 80-90% sample retention (R_{total}), with 80-90% of that sample being digitized as individual samples (f_{total}). Design modifications of the main channel (*e.g.*, the use of constrictions in the main channel before and after each well) and tapering the bottom wells in the direction of the sample flow improved the breakup of sample volumes and gave rise to nearly 100% in R_{total} and f_{total}. Furthermore, these results were not limited in scale-up. Bottom-well SD chips with up to 38,400 wells (V_w = 2 nL) permitted digitization of over 75 BL of sample into individual droplets per chip. These results provide an important foundation for various applications which range from enzymatic studies, where samples are derived from single live cells, to large-scale biochemical studies (*e.g.*, drug screening assays).

Acknowledgments

We gratefully acknowledge support of this work by the National Science Foundation (CHE0844688) and the National Institutes of Health (GM103459).

References

1. Anna SL, Bontoux N, Stone HA. Appl. Phys. Lett. 2003; 82:364–366.
2. Garstecki P, Fuerstman MJ, Stone HA, Whitesides GM. Lab Chip. 2006; 6:437–46. [PubMed: 16511628]
3. Song H, Tice JD, Ismagilov RF. Angew. Chem. Int. Ed. 2003; 42:768–72.
4. Cordero ML, Rolfsnes HO, Burnham DR, Campbell PA, McGloin D, Baroud CN. New J. Phys. 2009; 11:075033.
5. Vijayakumar K, Gulati S, deMello AJ. Edel, J. B. Chem. Sci. 2011; 1:447–452.
6. Abate AR, Weitz DA. Lab Chip. 2011; 11:1911–1915. [PubMed: 21505660]
7. Edgar JS, Pabbati CP, Lorenz RM, He M, Fiorini GS, Chiu DT. Anal. Chem. 2006; 78:6948–54. [PubMed: 17007519]
8. Edgar JS, Milne G, Zhao Y, Pabbati CP, Lim DS, Chiu DT. Angew. Chem. Int. Ed. 2009; 48:2719–22.
9. He M, Edgar JS, Jeffries GD, Lorenz RM, Shelby JP, Chiu DT. Anal. Chem. 2005; 77:1539–44. [PubMed: 15762555]
10. Koster S, Angile FE, Duan H, Agresti JJ, Wintner A, Schmitz C, Rowat AC, Merten CA, Pisignano D, Griffiths AD, Weitz DA. Lab Chip. 2008; 8:1110–5. [PubMed: 18584086]
11. Huebner A, Srisa Art M, Holt D, Abell C, Hollfelder F, deMello AJ, Edel JB. Chem. Commun. 2007:1218–20.
12. Clausell-Tormos J, Lieber D, Baret JC, El-Harrak A, Miller OJ, Frenz L, Blouwolff J, Humphry KJ, Koster S, Duan H, Holtze C, Weitz DA, Griffiths AD, Merten CA. Chem. Biol. 2008; 15:427–37. [PubMed: 18482695]
13. Shim JU, Olguin LF, Whyte G, Scott D, Babtie A, Abell C, Huck WT, Hollfelder FJ. Am. Chem. Soc. 2009; 131:15251–6.
14. Zeng Y, Novak R, Shuga J, Smith MT, Mathies RA. Anal. Chem. 2010; 82:3183–90. [PubMed: 20192178]
15. Agresti JJ, Antipov E, Abate AR, Ahn K, Rowat AC, Baret JC, Marquez M, Klibanov AM, Griffiths AD, Weitz DA. Proc. Natl. Acad. Sci. U. S. A. 2010; 107:4004–9. [PubMed: 20142500]
16. Novak R, Zeng Y, Shuga J, Venugopalan G, Fletcher DA, Smith MT, Mathies RA. Angew. Chem. Int. Ed. Engl. 2010; 50:390–5. [PubMed: 21132688]
17. Hufnagel H, Huebner A, Gülch C, Güse K, Abell C, Hollfelder F. Lab Chip. 2009; 9:1576–1582. [PubMed: 19458865]
18. Boedicker JQ, Li L, Kline TR, Ismagilov RF. Lab Chip. 2008; 8:1265–72. [PubMed: 18651067]

19. Brouzes E, Medkova M, Savenelli N, Marran D, Twardowski M, Hutchison JB, Rothberg JM, Link DR, Perrimon N, Samuels ML. Proc. Natl. Acad. Sci. U. S. A. 2009; 106:14195–200. [PubMed: 19617544]
20. Huebner A, Sharma S, Srisa Art M, Hollfelder F, Edel JB, Demello AJ. Lab Chip. 2008; 8:1244–54. [PubMed: 18651063]
21. Chiu DT, Lorenz RM. Acc. Chem. Res. 2009; 42:649–58. [PubMed: 19260732]
22. Chiu DT, Lorenz RM, Jeffries GD. Anal. Chem. 2009; 81:5111–8. [PubMed: 19507850]
23. Pompano RR, Liu W, Du W, Ismagilov RF. Annu. Rev. Anal. Chem. 2011; 4:59–81.
24. Schneider T, Kreutz J, Chiu DT. Anal. Chem. 2013; 85:3476–82. [PubMed: 23495853]
25. Cohen DE, Schneider T, Wang M, Chiu DT. Anal. Chem. 2010; 82:5707–5717. [PubMed: 20550137]
26. Gansen A, Herrick AM, Dimov IK, Lee LP, Chiu DT. Lab Chip. 2012; 12:2247–54. [PubMed: 22399016]
27. Burnham DR, Schneider T, Chiu, D. T. Proc. SPIE. 2010; 7762:77621T.
28. Gosse C, Croquette V. Biophys. J. 2002; 82:3314–29. [PubMed: 12023254]
29. Pamme N. Lab Chip. 2007; 7:1644–59. [PubMed: 18030382]
30. Zborowski, M. Magnetic cell separation. Zborowski, M.; Chalmers, JJ., editors. Elsevier; Amsterdam: 2007. p. 105-118.
31. Song JW, Gu W, Futai N, Warner KA, Nor JE, Takayama S. Anal. Chem. 2005; 77:3993–9. [PubMed: 15987102]
32. Xia Y, Whitesides GM. Annu. Rev. Mater. Sci. 1998; 28:153–184.
33. Yen GS, Fujimoto BS, Schneider T, Huynh DTK, Jeffries GDM, Chiu DT. Lab Chip. 2010; 11:974–977. [PubMed: 21229183]
34. Klinger, T. Image processing with LabVIEW and IMAQ vision. Vol. 1. Prentice Hall PTR; Upper Saddle River, NJ: 2003. p. 319

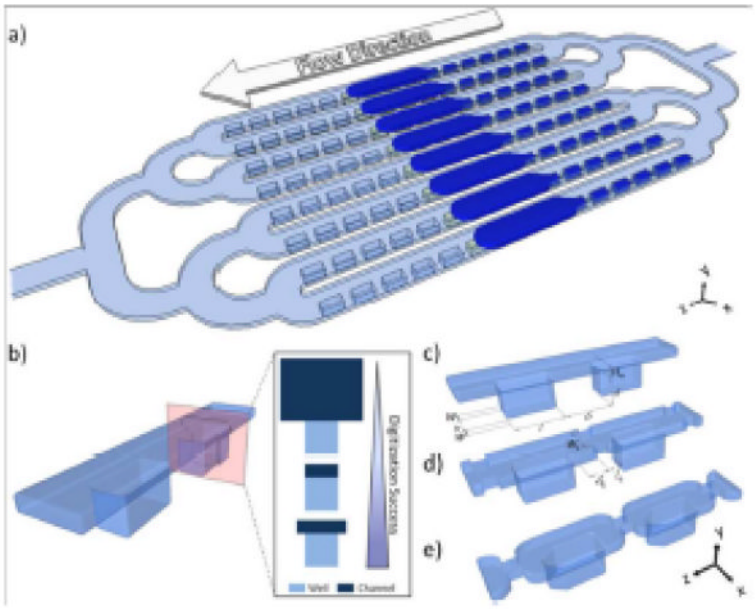

Figure 1.

Self-Digitization in microfluidic bottom well chips for small volume biochemical analyses (e.g., PCR): a) Scheme of sample digitization in a bottom-well SD chip with parallel rows of bottom wells connected by a main channel. b) Sketch of well-channel cross-sectional design and the associated digitization success (not to scale). d-e) Design evolution of the main channel geometry from straight (c) to constricted main channels (d, e) and modification of the well geometry (e) to maximize sample digitization and retention. The dimensions of the channels are defined by a main channel height, H_m, and width of $W_{main} = w + 2W$, wherein w is the width of the bottom well and W is the overhang of the main channel measured perpendicular to the flow direction (measured in the × – direction). Bottom wells of width, length and depth ($w \times l \times d$) are spaced apart by δ or separated by a constriction of width, W_c, and length, l_c, placed at a distance of δ_c before and after each well.

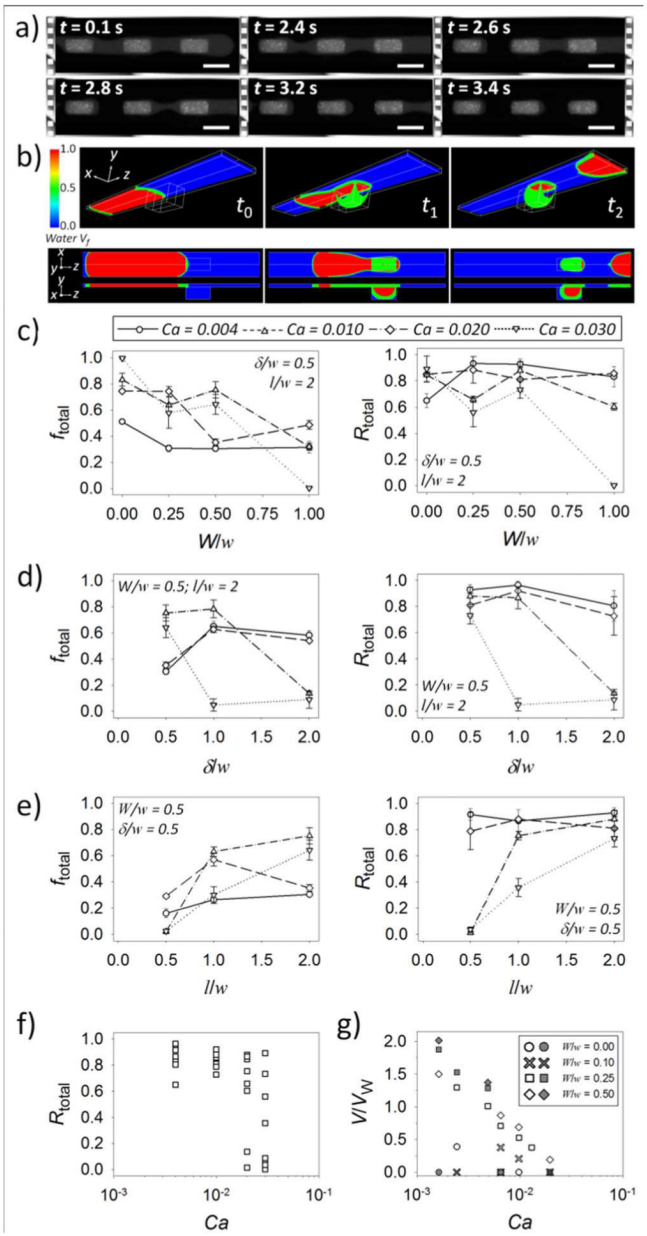

Figure 2.

Sample digitization shown by fluorescence microscopy and CFD. a) Fluorescence image sequence of sample digitization in a 1,024-well chip at $Ca = 0.015$. Shown is the shearing of an aqueous sample (supplemented with fluorescein) by 50 cSt silicone oil with 0.01% w/w Gransurf 77 in three wells imaged at the *x*-*z*-midplane. Note the nicking of the aqueous phase between wells before digitization from the bulk aqueous solution. Scale bar corresponds to 200 μm. b) Example of well filling by 3-dimensional water-in-oil multiphase flow CFD analysis before (t_0), during (t_1), and after droplet breakup (t_2); shown are the color contours in isometric, top, and side view at the *x*-*z*- and *y*-*z*-midplane of the water volume fraction ranging from blue = oil to red = water and the water/oil-interface shown as an isosurface (green). The flow in a) and b) is from left to right. Summary of variations in c) normalized main channel overhang (W/w), d) normalized inter-well spacing (δ/w), and e)

the well aspect ratio with respect to the flow direction (l/w) and its effect on the filling efficiency (f_{total}) and sample retention ratio (R_{total}). The studies were conducted in chips with 20 μm tall (H_m) main channels with wells below them. Data are shown as mean ± SD (n = 2). f) combined results showing the trend of sample retention in wells with respect to Ca from on chip studies with 1,024 wells based on R_{total} and g) results from a parametric CFD study with different H_m (white symbols = 25 μm, grey symbols = 50 μm). Note the distinct cutoff in sample retention above $Ca > 0.02$ in (g) and the similarity in retention cutoff (Ca) between f) and g) despite the difference in data used (area vs. volume of retained sample; see main text).

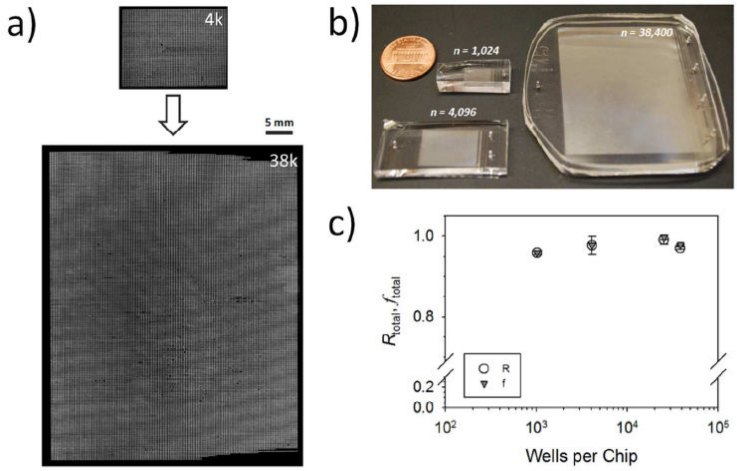

Figure 3.
Effect of scale up from 4,096 to 38,400 wells per chip. a) Fluorescent images of digitized samples in microfluidic bottom well chips with 2-nL wells and b) Photographs of the chip scale-up. c) Summary of retention and digitization efficiency. Data are shown as mean ± SD (n = 2).